

Magnetic structure and phase stability of the van der Waals bonded ferromagnet $\text{Fe}_{3-x}\text{GeTe}_2$

Andrew F. May,^{1,*} Stuart Calder,² Claudia Cantoni,¹ Huibo Cao,² and Michael A. McGuire¹

¹*Materials Science and Technology Division, Oak Ridge National Laboratory, Oak Ridge, TN 37831*

²*Quantum Condensed Matter Division, Oak Ridge National Laboratory, Oak Ridge, TN 37831*

(Dated: March 30, 2025)

The magnetic structure and phase width of the layered ferromagnetic compound Fe_3GeTe_2 has been investigated by a combination of synthesis, x-ray and neutron diffraction, high resolution microscopy, and magnetization measurements. Single crystals were synthesized by self-flux reactions, and single crystal neutron diffraction finds ferromagnetic order with moments of $1.11(5)\mu_B/\text{Fe}$ aligned along the c -axis at 4 K. These flux-grown crystals have a lower Curie temperature T_C compared to crystals previously grown by vapor transport, with T_C being suppressed from 230 K to approximately 150 K. Aided by the synthesis and characterization of a series of polycrystalline samples, T_C is found to correlate with Fe concentration where Fe-deficiency reduces T_C . A phase boundary exists near approximately $\text{Fe}_{2.7}\text{GeTe}_2$, and occupation of an interlayer position may allow compositions such as $\text{Fe}_{3.05}\text{GeTe}_2$ to form. However, for our Fe-deficient single crystals, Fe atoms within the van der Waals gap were not detected by high resolution electron microscopy or single crystal diffraction. In addition, Hall effect and thermoelectric measurements on flux-grown crystals suggest multiple carrier types contribute to electrical transport in $\text{Fe}_{3-x}\text{GeTe}_2$ and structurally-related $\text{Ni}_{3-x}\text{GeTe}_2$.

I. INTRODUCTION

Fe_3GeTe_2 is a crystallographically-layered material, with ferromagnetism occurring below a Curie temperature of $T_C=230$ K.¹ It has a relatively new crystal structure, being first reported in 2006 along with the non-magnetic analogue Ni_3GeTe_2 .¹ Fe_3GeTe_2 contains Fe_3Ge slabs separated by van der Waals bonded Te layers, as shown in Fig. 1. In addition to potentially being an itinerant ferromagnet,² the layered structure of Fe_3GeTe_2 makes it of interest from the perspective of ultra-thin materials production and characterization. Given the recent work demonstrating monolayer production via exfoliation of other van der Waals bonded chalcogenides, such as WSe_2 and MoS_2 ,^{3,4} it may be possible to generate mono-layers of Fe_3GeTe_2 to study the influence of dimensionality on magnetism. Indeed, this material appears to be relatively stable in air and is found to be easily cleaved by a blade.

Following the initial reports on polycrystalline samples in 2006, single crystals were grown by iodine-assisted vapor transport and reported in 2013.² Using a modified Arrott plot and other physical property measurements, a Curie temperature of 220 K was determined for these single crystals, which is slightly less than that reported for the polycrystalline material.^{1,2} Anisotropic magnetization measurements on the single crystals suggest that the c -axis is the easy axis, and an anisotropy field of at least 5 T was demonstrated at 10 K.² The spontaneous magnetization was derived to be $1.6\mu_B/\text{Fe}$ at 0 K, and from the calculated Rhodes–Wohlfarth ratio it was suggested that the magnetism is itinerant.² We note that the temperature dependence of the magnetization below T_C was somewhat irregular for the vapor transport grown crystals, and the microscopic magnetic structure has not been confirmed or measured by other tools such as neu-

tron diffraction.

The Fe_3GeTe_2 structure can be derived from that of Fe_{2-x}Ge , which possesses a three-dimensional framework built of hexagonal Ge-Fe(2) (ordered) nets connected by chains of Fe(1) that pierce each hexagon. A Curie temperature $T_C=485$ K has been reported for $\text{Fe}_{1.67}\text{Ge}$,⁵ and T_C varies with Fe concentration in the binary.⁶ In Fe_3GeTe_2 , a van der Waals bonded Te-Te layer divides the structure of Fe_{2-x}Ge into separate Fe_3Ge layers (see Fig. 1). The resulting structure is highly anisotropic, and contains Fe(1)-Fe(1) pairs across the hexagonal network built by Ge-Fe(2). Both compounds have the hexagonal space group $P6_3/mmc$ (no. 194), though the symmetry of this $\beta\text{-Fe}_{2-x}\text{Ge}$ has been brought into question for large vacancy concentrations x .⁷

In Fe_3GeTe_2 , the Fe(2) position was reported to have a small concentration of vacancies (17%) based on refinement of single crystal x-ray diffraction data, but chemical characterization suggested the composition is Fe_3GeTe_2 .¹ Interestingly, the majority of vacancies in Fe_{2-x}Ge are also located on the chemically similar Fe(2) position (Wyckoff 2d site), and a very wide (and complex) phase width is observed.⁶ At the congruently-melting composition $\text{Fe}_{1.67}\text{Ge}$, this site is only two-thirds occupied causing each Ge to have two bonds on average. A modest phase-width is therefore expected in Fe_3GeTe_2 based on the published crystallographic data, the intermetallic nature of this compound, and similarities to binary Fe_{2-x}Ge compounds. Furthermore, we expect the magnetic properties of Fe_3GeTe_2 to be sensitive to Fe content.

We report the growth of single crystals via a molten flux technique that produces large, high-quality crystals. Single crystal neutron diffraction data indicate an ordered moment of $1.11(5)\mu_B/\text{Fe}$ along the c -axis at 4 K. The investigation of our single crystals was complemented by the synthesis and characterization of a series of

polycrystalline samples that contain varying Fe concentrations. The lattice parameters and T_C vary smoothly with Fe concentration, and reduced Fe content leads to lower T_C . We also present a detailed analysis of the structural and physical properties of our $\text{Fe}_{3-x}\text{GeTe}_2$ crystals, which are mildly itinerant ferromagnets that are found to possess multi-carrier electronic transport.

II. EXPERIMENTAL DETAILS

Single crystals were grown from Fe-Ge-Te ‘self’-fluxes, and a melt composition of Fe_2GeTe_4 produced the largest crystals of those investigated. Crystals were also successfully grown from the compositions FeGe_2Te_4 and FeGeTe_2 using similar heating procedures, though these crystals were typically smaller and had slightly lower Curie temperatures. High purity elements from Alfa Aesar (Fe 99.98%, Ge 99.9999%, and Te 99.9999%) were combined in Al_2O_3 crucibles and sealed in evacuated quartz ampoules. A crucible filled with quartz wool was placed on top of the growth crucible to catch the excess flux during centrifugation. The melt was homogenized at 950°C for approximately 12 h, then cooled slowly to 675°C , at which temperature the ampoules were removed from the furnace and placed in a centrifuge to expel the excess flux. A variety of cooling rates were found to produce crystals, and in this paper we report data from crystals obtained after cooling at 1 and $3^\circ/\text{h}$ (the properties were observed to be equivalent). We also synthesized crystals of Ni_3GeTe_2 to provide a non-magnetic reference material during our investigation of transport properties.

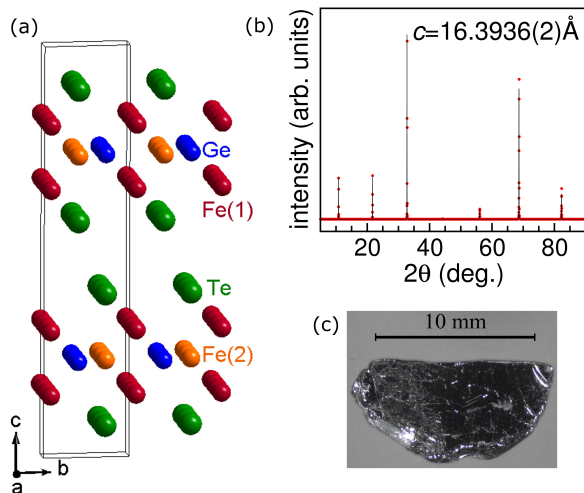


FIG. 1. (color online). (a) Image of crystal structure with atomic positions labeled; Fe(1)-Fe(1) bonds pierce the center of each hexagon formed by Fe(2)-Ge. (b) X-ray diffraction data for an as-grown facet of Fe_3GeTe_2 showing the c -axis normal with exclusively 00l diffraction peaks observed; a Le Bail fit (solid line) yielded the c -axis lattice parameter shown in the image. (c) A picture of a large single crystal.

Crystals of Ni_3GeTe_2 were grown from a melt of NiGeTe_2 cooled at $3^\circ/\text{h}$, with the flux removed at 660°C . The crystals of Ni_3GeTe_2 were generally smaller than those of Fe_3GeTe_2 .

Polycrystalline samples with nominal Fe concentrations between $\text{Fe}_{3.10}\text{GeTe}_2$ and $\text{Fe}_{2.60}\text{GeTe}_2$ were prepared by grinding Fe powder, Ge powder, and Te shot in a He filled glove box. The mixture was transferred, under He, to a vacuum line where the quartz ampoule was sealed under vacuum. The samples were heated at 675°C for approximately 10 d. The as-reacted $\text{Fe}_{3-x}\text{GeTe}_2$ samples were found to be either slightly sintered and dull black for small x , or heavily sintered with visible grain growth/crystallization for large x . At this point, the samples were analyzed with x-ray diffraction and magnetization measurements. Small pellets were then fired briefly at 600°C to facilitate isothermal magnetization and energy dispersive spectroscopy (EDS) measurements. EDS measurements were performed using a Bruker Quantax 70 EDS system on a Hitachi TM-3000 microscope.

Crystals from the flux-grown reactions are much larger than those needed for single crystal x-ray diffraction, and the process of cutting or crushing the crystals induces significant damage. Therefore, a small crystal from the polycrystalline reaction with nominal composition $\text{Fe}_{2.75}\text{GeTe}_2$ was selected for single crystal x-ray diffraction. Data were collected at 173 K on a Bruker SMART APEX CCD, using Mo- $K\alpha$ radiation ($\lambda = 0.71073\text{\AA}$). For refinement of the crystal structure, absorption corrections were applied with SADABS and SHELXL-97 was used to refine the data, and the atomic coordinates were standardized with Structure Tidy within PLATON.⁸⁻¹⁰ The refinement utilized 138 unique reflections from 1885 reflections and 12 refinement parameters. The Goodness of fit was 1.303 while $R_{\text{int}} = 0.0280$. Powder x-ray diffraction data were collected using a PANalytical X’Pert Pro MPD with a Cu $K_{\alpha,1}$ monochromator, and corresponding Le Bail and Rietveld refinements were performed using FullProf.¹¹

Magnetization measurements were performed in a Quantum Design Magnetic Property Measurement System, as well as with the AC Magnetic Susceptibility Option on a Quantum Design Physical Property Measurement System (PPMS). A PPMS was also used to measure the Seebeck coefficient, thermal conductivity and electrical resistivity using the Thermal Transport Option. For this measurement, gold-coated copper leads were attached to the sample using H20E Epo-Tek silver epoxy. Hall effect measurements and magnetoresistance measurements were performed using a standard four-point configuration with Pt wires attached via silver paint (DuPont 4929N). The Hall resistance ρ_H was obtained via the odd-in- \mathbf{H} part of the transverse resistance $\rho_H = (\rho_{xy}[\mathbf{H}] - \rho_{xy}[-\mathbf{H}])/2$ with maximum magnetic fields of magnitude $\mu_0 H = 8\text{ T}$ applied along the c -axis. Magnetoresistance was obtained from the even-in- \mathbf{H} portion of the longitudinal resistance with fields applied along the c -axis. At 2 K and 8 T, the magnetoresis-

tance was less than 2% and we have excluded the data from the manuscript.

To probe the microscopic crystal and magnetic structure, we performed single crystal neutron diffraction on the Four-circle instrument (HB-3A) at the High Flux Isotope Reactor (HFIR), ORNL. A single crystal of approximate dimensions 4 mm \times 4 mm was mounted on an Al rod inside a CCR. Using a wavelength of 1.003 Å, measurements were performed between 4 K and room temperature. A large number of reflections were collected at 220 K and 4 K to determine the nuclear and magnetic structures, respectively, which were refined with the program FullProf.¹¹

High resolution scanning transmission electron microscopy (STEM) was performed using a Nion Ultra-STEM200 microscope operating at 200 keV, equipped with a Gatan Enfium spectrometer for the in situ collection of electron energy loss spectra (EELS). Samples were examined in both plan view and cross-sectional orientations. Samples were prepared by a combination of polishing and Ar⁺ ion milling using a voltage of 2 keV. Contact with moisture was avoided during sample preparation.

III. RESULTS AND DISCUSSION

The single crystals obtained from self-flux growths are thin plates with dimensions reaching greater than 1 cm (see Fig. 1). X-ray diffraction data collected from the surface of as-grown facets confirm the expected orientation with [001] normal to the facet, as shown in Fig. 1. A Le Bail fit to the diffraction data in Fig. 1 yielded $c=16.3936(2)$ Å. Rietveld refinement of data collected on ground crystals resulted in $a=3.9535(7)$ Å and $c=16.396(2)$ Å. These values differ sharply from those in the literature, where $a=3.9910(10)$ Å and $c=16.336(3)$ Å were reported from room temperature single crystal x-ray diffraction.¹

Ni₃GeTe₂ crystals were grown from a self-flux to provide a non-magnetic reference material during the characterization of physical properties. The lattice parameters obtained for our Ni₃GeTe₂ crystals also differ from those in the literature, with refinement of powder diffraction data yielding $a=3.8372(2)$ Å and $c=16.0477(6)$ Å. This compares to $a=3.9110(10)$ Å and $c=16.022(3)$ Å previously reported for crystals with a composition of Ni_{2.95}GeTe₂ obtained from refinement of single crystal x-ray diffraction data.¹ Thus, for both Fe₃GeTe₂ and Ni₃GeTe₂ grown from a self-flux, the a lattice parameter is smaller and the c lattice parameter is slightly larger than the literature reports for crystals obtained from nominal 3-1-2 compositions (formed via solid state reactions).

In addition to having different lattice parameters than those in the literature, the flux-grown Fe₃GeTe₂ crystals have lower Curie temperatures than those previously reported for Fe₃GeTe₂. The crystals were grown

from self-fluxes, which minimize the chance for extrinsic doping. We thus speculated that Fe₃GeTe₂ contains a non-trivial phase width that influences structure and physical properties. Our EDS results suggest Fe and Ge deficiencies may exist, with a composition of Fe_{2.91(3)}Ge_{0.95(4)}Te_{2.00(4)} obtained. For the Ni-based analogue, EDS yielded Ni_{2.40(4)}Ge_{1.01(3)}Te_{2.00(3)} for crystals grown from NiGeTe₂.

To investigate the phase width of Fe_{3-x}GeTe₂, polycrystalline samples were produced via solid-state reactions with nominal compositions Fe_{3-x}GeTe₂ with $-0.1 \leq x \leq 0.4$. These materials were characterized using powder x-ray diffraction, EDS, and magnetization measurements. We begin by presenting the results of our crystallographic studies, and then return to the magnetic properties and detailed characterization of our single crystals. When necessary for unit conversion, we have utilized compositions obtained by Rietveld refinement. When discussing single crystals, we present data for crystals grown from Fe₂GeTe₄ melts, and refer to these by the composition obtained from refinement of single crystal neutron diffraction data, Fe_{2.76}Ge_{0.94}Te₂.

A. Structure and Composition

All polycrystalline samples were found to be phase pure within the limits of our powder x-ray diffractometer, with the exception being a sample of nominal composition Fe_{2.60}GeTe₂. This sample contained GeTe and FeTe₂ impurities, and data for this sample have been excluded from the manuscript. Our results thus suggest the Fe-deficient phase boundary is likely reached near Fe_{2.7}GeTe₂. We have not investigated the phase width with regard to Te or Ge.

The phase may accommodate some excess Fe beyond Fe₃GeTe₂, as the sample of nominal composition Fe_{3.10}GeTe₂ did not possess any obvious impurities by x-ray diffraction. The refined composition for this sample is Fe_{2.97(2)}GeTe₂, while large-area (300 μm diameter) EDS scans yielded Fe_{3.07(2)}Ge_{0.92(2)}Te_{2.00(2)}. The EDS results are likely influenced by minor secondary phases that are not detected by x-ray diffraction. An Fe-rich impurity was detected in back scattered electron images, and we were not able to isolate large grains of the main phase for EDS due to resolution limits. Therefore, we focus on compositions obtained from Rietveld refinements of the powder diffraction data. In the structurally-similar Ni₃GeTe₂ compound, occupation of an interlayer Ni(3) position at (0,0,0) was detected by single crystal x-ray diffraction, though occupation of this site was not observed in Fe₃GeTe₂.¹ We performed refinements including the hypothetical Fe(3), and the results suggest that an occupation of 3(1)% may exist for the nominal Fe_{3.10}GeTe₂. This result seems reasonable, but it is dependent on the range of data analyzed (in part due to a connection to the refinement of sample texture). Based on our single crystal diffraction and electron microscopy,

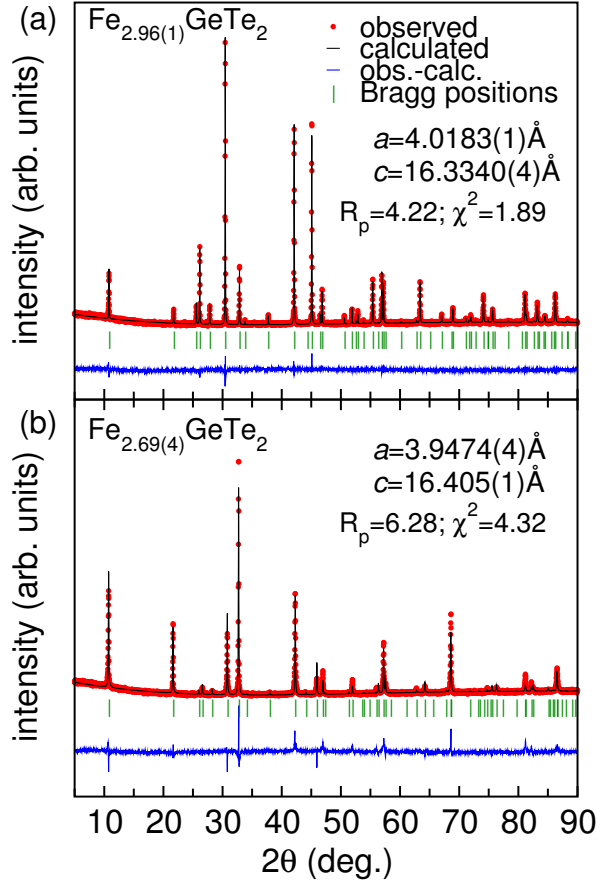


FIG. 2. (color online). Powder x-ray diffraction data for two polycrystalline samples with refined lattice parameters and compositions provided.

discussed below, we feel confident that there is not any significant occupation of this interlayer site in the nominally Fe-deficient samples (at least for $x \approx 0.25$). We therefore utilized the published crystal structure, with two Fe positions, to refine our diffraction data and report compositions based on this refinement.

Figure 2 presents powder diffraction data and Rietveld refinements for samples of nominal composition $\text{Fe}_{3.00}\text{GeTe}_2$ and $\text{Fe}_{2.75}\text{GeTe}_2$, which refined to the compositions $\text{Fe}_{2.96(1)}\text{GeTe}_2$ and $\text{Fe}_{2.69(4)}\text{GeTe}_2$, respectively. The lattice parameters obtained from refinement of the data in Fig. 2 confirm that the Fe-deficient sample has smaller a and larger c than the Fe-rich sample. This trend is shown in Fig. 3 for all polycrystalline samples, where the normalized lattice parameters are plotted as a function of Fe content. Data obtained from single-crystal x-ray diffraction (sc-xrd) are also included to confirm this behavior; note that the sc-xrd data were collected at 173 K where slightly smaller lattice parameters are expected. The increase in a with increasing Fe may be expected, with the lattice expanding as Fe(2) vacancies are filled. Indeed, a similar trend in a occurs for Fe_{2-x}Ge in the range $0.15 < x < 0.7$, where c was found to increase

with increasing Fe content.⁶

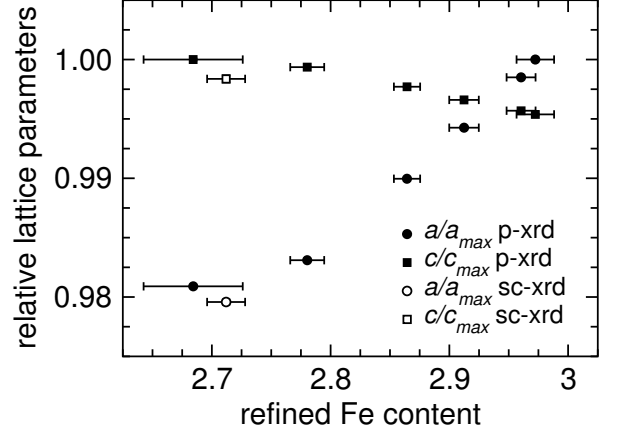


FIG. 3. Normalized lattice parameters as a function of refined Fe content for $\text{Fe}_{3-x}\text{GeTe}_2$ samples (powder x-ray diffraction ‘p-xrd’ at room temperature), including results obtained from single crystal x-ray (‘sc-xrd’) diffraction data collected at 173 K; $a_{\text{max}} = 4.0243(1)$ Å and $c_{\text{max}} = 16.405(1)$ Å. Vertical error bars are smaller than the size of the data markers.

Given the layered structure, we expect the greatest influence of the increased occupation of Fe(2) to be observed within the (Fe_3Ge) planes. Indeed, the relative expansion of a is greater than the relative contraction of c (see Fig. 3). We therefore expect the changes in c to be driven by the changes in a . That is, the decrease in c is due to an expansion of the basal plane that allows Te atoms to get closer to the Fe_3Ge layer, while increased occupation of Fe(2) also leads to greater Fe(2)-Te bonding. Consistent with this, Fe(2)-Te bond distances are smallest in the Fe-rich samples, as are Fe(1)-Fe(1) bond distances. As a result of Te being pulled towards the Fe_3Ge layers, the structure collapses along c to maintain the van der Waals bonds (the distance of which increases with increasing Fe). If the hypothetical Fe(3) becomes occupied at high Fe concentrations, its presence could lead to increased bonding that would also reduce c . However, refinements with Fe(3) reveal a larger Fe(3)-Te bond distance for higher Fe contents, suggesting that Fe(3) does not play a role in the contraction of c .

We note that the occupancy of Fe(2) is correlated to the refinement of texture (preferred orientation) in the powder diffraction data. In these samples, the texture physically increases with decreasing Fe content. This trend can be observed visually, with the Fe-deficient samples demonstrating more grain growth during the reaction. Not refining the texture results in much larger residuals, and thus the preferred orientation was refined for all samples and care was taken to minimize the texture during sample preparation. The main result is not strongly influenced by this, though, and the nominal composition clearly influences the amount of Fe in the final specimen and the trends are consistent. Also, to simplify the refinement, we did not allow Ge content to vary and fixed an overall displacement parameter.

The potential existence of interlayer Fe is important beyond understanding the modifications to the lattice with changing Fe content. As shown below, the total Fe content clearly influences the magnetic properties and interlayer Fe could play a particularly important role in determining the saturation magnetization and coercive field. In regards to the chemistry and structure of these materials, the existence of interlayer Fe would imply a more three-dimensional material. As such, interlayer Fe would likely impede the production of thin-layers by cleaving bulk crystals. Similarly, if an amount of interlayer Fe can be controlled, it would likely influence the anisotropy of the electronic and magnetic properties. Interestingly, as discussed below, the samples with the highest Fe content have the largest anisotropy in the magnetic properties. While our powder diffraction results suggest Fe(3) is not occupied, we felt that additional investigation was warranted.

We investigated the issue of interlayer Fe with single crystal x-ray and neutron diffraction, and electron microscopy. The refinement results from the x-ray diffraction data are shown in Table I, and we clearly observe the partial occupation of Fe(2) with a refined composition $\text{Fe}_{2.71(2)}\text{GeTe}_2$ (recall this is for a crystal obtained from the $\text{Fe}_{2.75}\text{GeTe}_2$ polycrystalline reaction; Ge vacancies were not observed). Electron density was not detected at an interlayer Fe(3) position, consistent with earlier work for crystals selected from a polycrystalline sample of nominal composition Fe_3GeTe_2 .¹ Our single crystal neutron diffraction on flux-grown crystals, discussed in more detail below, does not find any strong evidence for occupation of the Fe(3) position.

While not presented in detail here, we would like to mention that Ge has a rather large and anisotropic thermal displacement parameter due to its in-plane bonding to Fe at the partially occupied Fe(2) position. Due to the vacancies at Fe(2), Ge is reduced to almost 2 bonds on average at the edge of the phase boundary, and the thermal ellipsoids of Ge are very wide within the plane (see Supplemental Materials). Due to the large vacancy concentration in $\text{Fe}_{1.60}\text{Ge}_2$, it has been suggested that the Ge atoms actually move off of their site and the symmetry is potentially broken.⁷ Additional discussion of the single crystal x-ray diffraction refinement is presented in the Supplemental Materials.

TABLE I. Selected data from refinements of single crystal x-ray diffraction collected on a crystal from a reaction of nominal composition $\text{Fe}_{2.75}\text{GeTe}_2$. Atomic coordinates are Fe(1): $0, 0, z$; Fe(2): $\frac{1}{3}, \frac{2}{3}, \frac{1}{4}$; Te: $\frac{1}{3}, \frac{2}{3}, z$; Ge: $\frac{1}{3}, \frac{2}{3}, \frac{3}{4}$.

a (Å)	3.9421(9)
c (Å)	16.378(5)
R_1 (all data)	0.0461
wR_2 (all data)	0.1019
Goodness of fit	1.306
Fe(1) z coord.	0.1721(2)
Te z coord.	0.0900(1)
Fe(2) occupancy	0.71(2)

We also performed high resolution scanning transmission microscopy (STEM) to investigate the local structure. For imaging, we used the high angle annular dark field detector (HAADF), which yields a contrast nearly proportional to Z^2 (Z = atomic number) and is therefore better suited for imaging vacancies and interstitials, and cations with different atomic numbers.

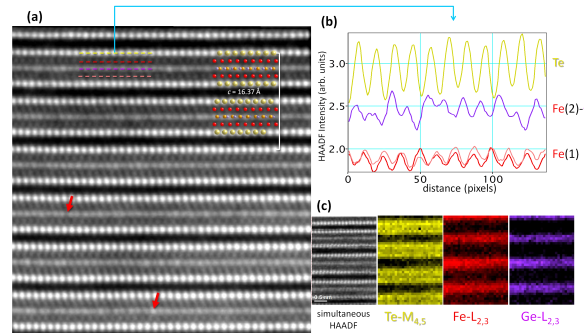


FIG. 4. (color online) HAADF STEM image showing Z -contrast. The heaviest columns (Te) show up as the brightest spots and Fe columns show up with the dimmest contrast. Van der Waals gaps are clearly visible as black stripes. The inset shows an overlay of the lattice projection along [130]. (b) Profiles of the intensity along the dashed lines shown in (a) indicating significant disorder in the Fe(2)-Ge plane. (c) EELS integrated intensity maps showing the chemical signature of the alternating Te, Fe, and Fe-Ge planes.

A representative cross-sectional image with the electron beam parallel to [130] is shown in Fig. 4(a), and plan view images with the electron beam parallel to [001] were also collected but are not shown. In general, the crystals looked to be of high quality, lacking obvious two or three dimensional defects. In the Z -contrast images, the van der Waals gaps between layers of Te atoms (brightest spots) can be easily identified and intensity is not observed between them, indicating that interlayer Fe is not present in our crystals. In both cross-sectional and plan view images, we observe a variation in the intensity of the atomic columns containing Fe(2) and Ge, which is consistent with the presence of Fe vacancies. The intensity profiles in Fig. 4(b) reveal these variations, with the Fe(2)-Ge columns displaying a clear disruption of the pattern expected for the case of fully occupied Fe(2) sites. Due to the difference in Z between Fe ($Z=26$) and Ge ($Z=32$), a fully occupied structure would display higher-intensity peaks adjacent to lower-intensity peaks in a high-low-high sequence when viewed down [130]. The red arrows in the image highlight Fe and Ge columns with markedly lower or higher intensity compared to average. Based on the images, we cannot exclude the possibility of Ge-Fe substitution or Ge vacancies in the Fe(2)-Ge planes. Due to the low vacancy concentration and the more delocalized nature of the EELS signal as compared to the HAADF signal, vacancies are not resolved in the EELS compositional maps shown in Fig. 4(c), which show a uniform

distribution for the integrated intensities of the Te- $M_{4,5}$, Fe- $L_{2,3}$ and Ge- $L_{2,3}$ edges.

The images were observed to change upon continued exposure to the electron beam. A movement of atoms and vacancies could be observed, with atoms eventually occupying the interlayer region and vacancies appearing to occupy sites besides Fe(2). In order to avoid beam-induced hopping and preserve observation of the intrinsic structure, images were collected rapidly on unirradiated regions by summing 20 frames, each one acquired within 1 s. EEL spectrum images were acquired using a spacing of 0.87 Å and a dwell time of 0.2 s. Beam-induced structural effects were also noted for Ni_3GeTe_2 in Ref. 1.

EELS was utilized to look for differences in the oxidation state of the two Fe sites. The ratio of the Fe $L_{3,2}$ peaks gives an indication regarding the oxidation state, though this can vary with details of the bonding environment. We find an $L_{3,2}$ ratio that varies slightly between the Fe(1) and Fe(2) positions, which may suggest the Fe atoms are in slightly different oxidation states or carry a different moment. We considered this effect when modeling our neutron diffraction data, but do not detect a large variation between the moments. Mössbauer spectroscopy would likely provide better insight into the magnetic behaviors of the different Fe positions.

The lack of evidence for occupation of Fe(3) in the STEM and diffraction studies may be due to the low-occupation of this position, which is likely to be further reduced with the overall decrease of Fe content in our samples due to the flux growth. Examination of Fe-rich crystals will offer the best chance for identifying interlayer Fe, if it exists, though even then the concentration will likely be very small and observation will be challenging. Even at such low concentrations, though, the presence of interlayer Fe could strongly influence the physical properties.

B. Single Crystal Neutron Diffraction

Single crystal neutron diffraction was performed on a crystal obtained from the Fe_2GeTe_4 flux. This flux composition was found to produce the largest crystals, and thus it was investigated in the most detail (including magnetization and transport measurements below). The crystal structure was refined using data collected at 220 K, and the magnetic structure was obtained from data collected at 4 K.

Figure 5 shows representative rocking curves obtained during the single crystal neutron diffraction data collection. As shown, there is strong temperature dependence that indicates the onset of magnetic ordering. The nuclear refinement is consistent with the single crystal and powder x-ray diffraction data. For the crystal investigated by neutron diffraction, we refine vacancies at the Fe(2) and Ge sites, and do not observe strong evidence for Fe substituting for Ge. Consistent with the above discussion, we do not detect any Fe between the Te-Te lay-

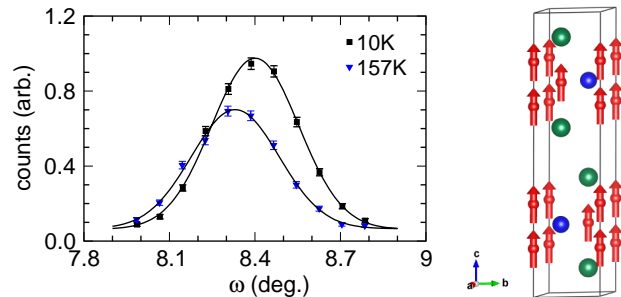


FIG. 5. (color online). Rocking curves of the 010 reflection from single crystal neutron diffraction on $Fe_{2.76}Ge_{0.94}Te_2$ at 10 K and 157 K. The solid lines are Gaussian fits to the peaks. The image on the right shows the magnetic structure obtained by refinement of neutron diffraction data collected at 4 K (Fe = red, Te = green, Ge = blue).

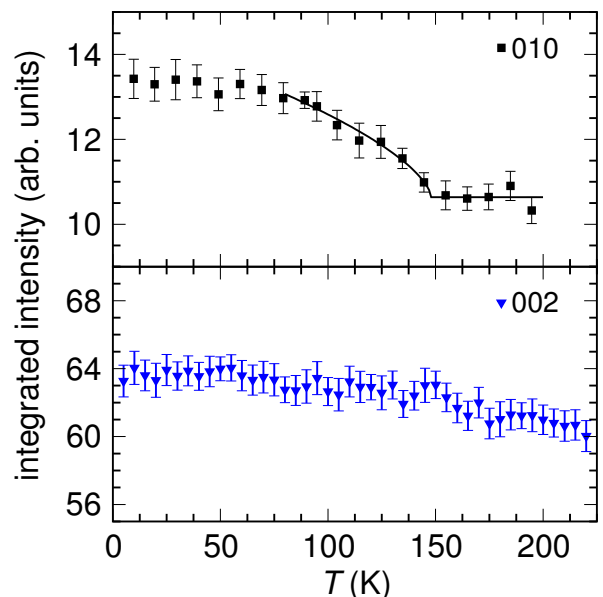


FIG. 6. (color online). Integrated intensities of Bragg peaks from single crystal neutron diffraction on $Fe_{2.76}Ge_{0.94}Te_2$. The increase in intensity for the 010 peak below T_C originates from the magnetic order along c , whereas the intensity of the 002 peak does not change significantly with temperature.

ers. The refined composition is $Fe_{2.76(4)}Ge_{0.94(4)}Te_2$ with $R_F=4.11$ and $\chi^2=0.423$. We then fixed these refinement parameters and refined only the magnetic components at low temperature.

An ordered moment along c of $1.11(5)\mu_B/Fe$ is obtained by refinement of the 4 K data, and a schematic of the magnetic structure is shown in Fig. 5. Our refinement does not indicate any significant difference in the moments on the two Fe positions. If we allow both moments to refine separately, we obtain $1.07(11)\mu_B/Fe(1)$ and $0.9(5)\mu_B/Fe(2)$. We note that the error on the moment value increases appreciably when both are allowed to refine separately and gives values consistent with that

for fixed Fe(1) and Fe(2). Thus, within the limits of this data, we have no reason to suspect that the different sites carry significantly different moments. For comparison, in $\text{Fe}_{1.76}\text{Ge}$ the ordered moments lie in the ab -plane, and an average moment of $1.56 \pm 0.2 \mu_B/\text{Fe}$ was reported based on neutron diffraction.¹² There has been contradictory reports regarding a variation of the moments between the two Fe sites in Fe_{2-x}Ge .¹²⁻¹⁴ The more recent Mössbauer results have suggested that a larger moment resides on the Fe(2) site, and perhaps similar experiments on Fe_3GeTe_2 may provide additional insight into the roles of the different Fe environments. The difference in the easy axis between Fe_3GeTe_2 and $\text{Fe}_{1.67}\text{Ge}$ is most likely caused by the increased chemical anisotropy associated with the inclusion of the Te-Te layer into the Fe_3GeTe_2 structure.

We confirmed the ferromagnetic ordering temperature and orientation of the moments by tracking the 010 and 002 Bragg peaks, as shown in Fig. 6. The power law fit between 80 K and 180 K in Fig. 6 yields $T_C = 148(3)$ K, which is consistent with the bulk magnetization measurements. The intensity of the 010 peak increases when the moments lie perpendicular to the 010 scattering vector. Therefore, the increase in intensity below ≈ 150 K shown in Fig. 6(a) demonstrates that the moments do not lie along the b -axis, and when combined with the temperature-independent behavior of 002 intensity we verify that the moments lie along c . This shows that there is not any significant spin canting or reorientation as temperature decreases. In addition, we did not observe any significant change in the nuclear structure across the magnetic ordering.

C. Magnetization

Magnetization measurements were performed on the polycrystalline materials to determine their Curie temperatures and correlate this with structure and composition. Results of these measurements are shown in Fig. 7(a), where refined Fe contents are used in the legend.

The data in Fig. 7(a) clearly demonstrate that the Curie temperature decreases with decreasing Fe content. The reduced T_C with increasing vacancies on the Fe(2) site may be caused by a disruption of the magnetic exchange with increasing disorder and magnetic dilution via vacancies. There may also be a structural component, though, as we observe that the reduced T_C correlates with the expansion of c , an increase in Fe(1)-Fe(1) bond distance, and decrease in Fe(1)-Fe(2) bond distances. A similar reduction in T_C is observed for Fe_{2-x}Ge materials as x increases, though, where a more typical decrease in the lattice parameters is observed with increasing x .⁶ Investigating the pressure-dependence of T_C or the anisotropy of the magnetic excitation spectra may provide further insight, as would theoretical calculations into the dependence of T_C on c .

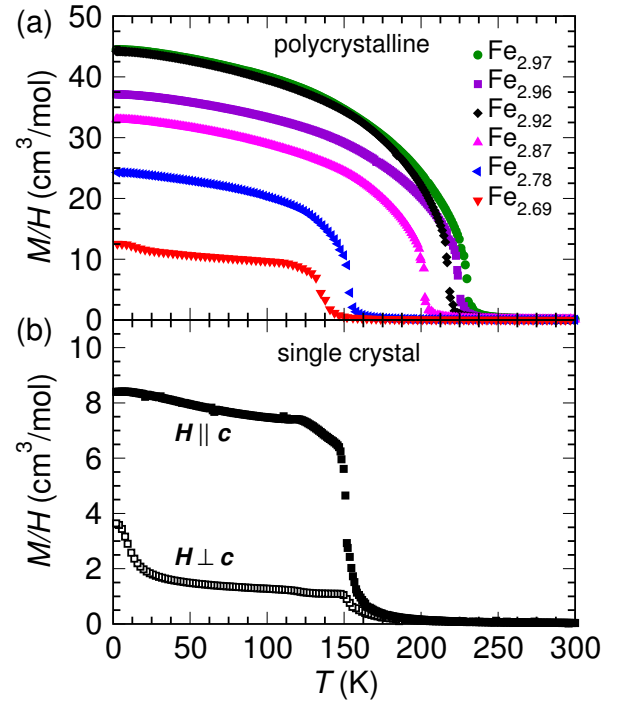


FIG. 7. (color online) (a) Temperature dependence of the magnetization for polycrystalline $\text{Fe}_{3-x}\text{GeTe}_2$ materials with various Fe concentrations as indicated by the refined Fe content in the legend, and (b) anisotropic magnetization of flux-grown $\text{Fe}_{2.76}\text{Ge}_{0.94}\text{Te}_2$. All data were collected upon cooling in an applied field of $\mu_0 H = 0.01$ T.

Anisotropic magnetization data for single crystalline $\text{Fe}_{3-x}\text{GeTe}_2$ are shown in Fig. 7(b). These data demonstrate that the easy axis for magnetization is along the crystallographic c -axis, which is consistent with our neutron diffraction and Ref. 2. The shape of $M(T)$ evolves with decreasing Fe content, changing from power-law behavior in the Fe-rich samples to a more abrupt and kink-containing curve in the Fe-deficient samples. The $M(T)$ data reported on the vapor transport crystals, with $T_C \approx 220$ K, has a temperature dependence similar to that shown in Fig. 7(b). Therefore, the non-power law behavior may be linked to domain wall formation and movement. It is certainly possible that different growth conditions produce different Fe(2)/Fe(3) contents, which also modify the properties independently. We also confirmed that $\text{Ni}_{3-x}\text{GeTe}_2$ appears to be a Pauli paramagnet.

Isothermal magnetization data are shown in Fig. 8. In panel (a), data for three polycrystalline samples are shown while panel (b) contains data for an oriented single crystal. The isothermal magnetization measurements for polycrystalline samples reveal some interesting trends with composition. It is clear that the Fe-deficient samples have a much lower remanent magnetization and very little coercivity. Also, the moment essentially saturates at high fields for the Fe-deficient samples while a linear rise with field is observed for the Fe-rich samples.

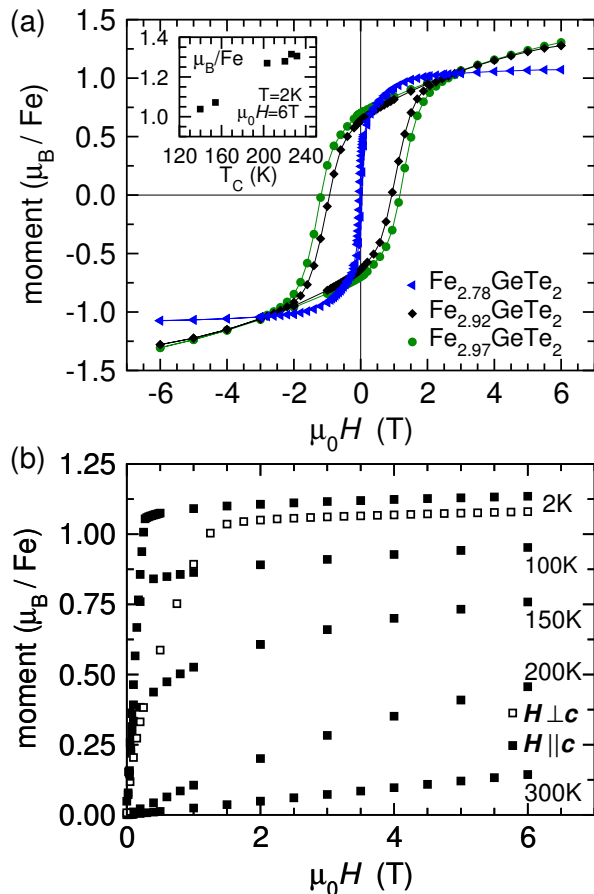


FIG. 8. (color online). (a) Magnetization loops at 2 K for three compositions of polycrystalline $\text{Fe}_{3-x}\text{GeTe}_2$ (refined values provided), and the inset shows the magnetization at 2 K and 6 T for polycrystalline samples. (b) Magnetization versus applied field for single crystalline $\text{Fe}_{2.76}\text{Ge}_{0.94}\text{Te}_2$ at various temperatures, with the anisotropy demonstrated at 2 K.

The linear increase at higher fields for $\text{Fe}_{2.97}\text{GeTe}_2$ may be related to an enhanced anisotropy of the saturation field at higher Fe content. Our low-Fe content crystals have an estimated anisotropy field of 1.5 T, as shown in Fig. 8(b). An anisotropy field of ≈ 5 T was observed at 10 K for crystals grown by vapor transport,² and the reported $T_C \approx 220$ K suggests a large Fe content in those crystals. The linear rise at large fields may also be from some paramagnetic ions, either an impurity or potentially interlayer Fe. We note that our $\text{Fe}_{2.76}\text{Ge}_{0.94}\text{Te}_2$ crystals did not reveal any unexpected behavior when measured to 12 T.

The ‘saturation magnetization’ of all polycrystalline $\text{Fe}_{3-x}\text{GeTe}_2$ samples is shown as an inset in Fig. 8(a) and values are listed in the summary of samples provided as Table II. The saturation magnetization is taken as the value of the magnetization (in μ_B/Fe) obtained at 2 K and 6 T (refined compositions are used for unit conversion). This does not represent a true saturation magnetization for all samples due to the linear increase

in M at large H . We clearly see that higher T_C (higher Fe content) correlates with larger induced moments for a given T at large applied fields. T_C was defined using the intercept of the steepest tangent. The effective moments determined from the susceptibility (χ) between 250 and 360 K were found to vary between $3.9(2)$ and $4.9(1)\mu_B/\text{Fe}$, with higher T_C generally corresponding to larger effective moments. We used a standard Curie-Weiss law ($\chi = C/(T - T_{CW})$) and fit data collected on cooling in an applied field of 0.1 T. Curie-Weiss temperatures T_{CW} obtained from these fits agreed well with the Curie temperatures obtained from measurements at lower fields.

We calculated the Rhodes-Wohlfarth ratio (RWR) for our polycrystalline samples. The RWR provides a quick means to characterize the degree to which a magnetic moment is localized. RWR is defined as $\text{RWR} = p_c/p_s$, with p_c obtained from the effective moment $p_c(p_c + 2) = p_{eff}^2$.^{15,16} Physically, p_c is the saturation moment expected from the effective moment in the paramagnetic phase and p_s is the saturation moment obtained in the ordered state. $\text{RWR} = 1$ for localized systems and is larger in an itinerant system, with the ratio increasing as T_C decreases. Here, we take p_s as the magnetization obtained at 2 K and 6 T and calculate RWR values between 2.7 and 3.4 for our polycrystalline samples. These values are fairly similar to the $\text{RWR} = 3.8$ reported in Ref. 2.

The observation of $\text{RWR} > 1$ in compounds with a low Curie temperature ($T_C \lesssim 500$ K) suggests itinerant ferromagnetism is likely present. In comparison to the values tabulated by Wohlfarth in 1978 and Moriya in 1979, these $\text{Fe}_{3-x}\text{GeTe}_2$ compounds lie in the region between localized and itinerant ferromagnetism.^{15,16} We do not observe a strong magnetoelastic effect at the transition, which is expected for large RWR (itinerant) systems.¹⁵ While we do not observe a strong increase in the RWR values as T_C decreases, this can likely be attributed to the influence of vacancies on the structure and magnetism (multiple effects influencing both T_C and RWR). Future measurements of the spin-waves via inelastic neutron scattering will aid in addressing the itinerant nature of this system, as would theoretical or experimental studies into the influence of pressure on T_C .

We have summarized the magnetization data as a plot correlating the lattice parameters with the Curie temperature, shown in Fig. 9. In addition, Table II provides a summary of the sample compositions determined using various methods as well as the magnetic properties. T_C clearly decreases as Fe vacancies are introduced and the lattice responds with a decrease in the in-plane lattice parameter and a slight expansion along c . Thus, Fig. 9 can be used along with Fig. 3 as a guide to predict the composition needed to obtain a particular T_C or as a means to expedite characterization. Figure 9 shows that the flux-grown crystals do not behave unexpectedly based on the behavior of polycrystalline materials.

TABLE II. Summary of samples and magnetic properties for polycrystalline $\text{Fe}_{3-x}\text{GeTe}_2$. Rietveld compositions originate in refinement of powder diffraction data while EDS values are for large area EDS analysis that may include impurities.

Fe composition			a	c	T_C	μ_{sat}	μ_{eff}	T_{CW}
nominal	Rietveld	EDS	(Å)	(Å)	(K)	(μ_B/Fe)	(μ_B/Fe)	(K)
3.10	2.97(2)	3.07(2)	4.0243(1)	16.3289(5)	232	1.31	4.9(1)	225.6(2)
3.00	2.96(1)	3.06(3)	4.0183(1)	16.3340(4)	226	1.32	4.8(1)	221.7(1)
2.90	2.92(1)	2.92(3)	4.0012(1)	16.3490(4)	220	1.28	4.4(1)	218.9(1)
2.85	2.87(1)	2.88(2)	3.9839(1)	16.3672(3)	203	1.27	4.4(1)	203.2(1)
2.80	2.78(1)	2.81(2)	3.9563(1)	16.3943(4)	154	1.08	4.5(1)	143.5(3)
2.75	2.69(4)	2.79(3)	3.9474(4)	16.405(1)	140	1.04	3.9(2)	142.6(2)

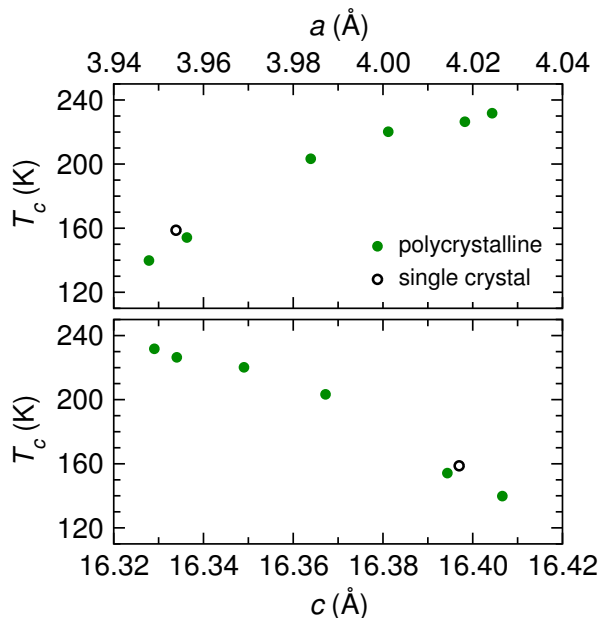


FIG. 9. (color online). Curie temperature as a function of lattice parameters for $\text{Fe}_{3-x}\text{GeTe}_2$.

D. Hall Effect and Seebeck Coefficients

We have utilized Hall effect and thermoelectric measurements to characterize the in-plane electrical transport in $\text{Fe}_{2.76}\text{Ge}_{0.94}\text{Te}_2$ and $\text{Ni}_{3-x}\text{GeTe}_2$ crystals. These results, summarized in Fig. 10, reveal that both systems likely have multiple carrier types contributing to conduction. We observe positive Hall coefficients and negative Seebeck coefficients, which would independently suggest p -type and n -type conduction, respectively. The linear dependence of the Hall resistance on applied field prohibits a detailed analysis aimed at determining the contribution of each band/carrier-type. Theoretical calculations would provide additional insight into the origin of this apparent multi-carrier transport. We note that our flux-grown crystals of $\text{Ni}_{3-x}\text{GeTe}_2$ likely have $x \approx 0.6$ based on EDS measurements.

At room temperature, the Hall coefficient R_H of $\text{Ni}_{3-x}\text{GeTe}_2$ is about an order of magnitude smaller than that of $\text{Fe}_{2.76}\text{Ge}_{0.94}\text{Te}_2$, which translates to a larger hole concentration in $\text{Ni}_{3-x}\text{GeTe}_2$ if a single-carrier model is

used. Specifically, at 300 K the Hall carrier density $n_H = 1/R_H e$ is approximately $1.8 \times 10^{22} \text{cm}^{-3}$ for $\text{Ni}_{3-x}\text{GeTe}_2$ and approximately $1.9 \times 10^{21} \text{cm}^{-3}$ for $\text{Fe}_{2.76}\text{Ge}_{0.94}\text{Te}_2$. If both holes and electrons are present, as suggested by these results, the Hall coefficients would be artificially reduced and the carrier concentrations reported would be upper-limits to the actual number of holes in the system. A more complete compensation of charge carriers may be responsible for the smaller Hall coefficient of $\text{Ni}_{3-x}\text{GeTe}_2$, though we found $\text{Ni}_{3-x}\text{GeTe}_2$ to have about an order of magnitude lower electrical resistivity (Supplemental Materials). As discussed in the Supplemental Materials, the Hall coefficient of $\text{Fe}_{2.76}\text{Ge}_{0.94}\text{Te}_2$ is strongly influenced by an anomalous Hall contribution below ≈ 200 K. Thermal conductivity and specific heat data for $\text{Fe}_{2.76}\text{Ge}_{0.94}\text{Te}_2$ and $\text{Ni}_{3-x}\text{GeTe}_2$ are also presented in the Supplemental Materials.¹⁷

IV. CONCLUSIONS

We find that Fe_3GeTe_2 and Ni_3GeTe_2 support a modest phase width with respect to transition metal content. In ferromagnetic $\text{Fe}_{3-x}\text{GeTe}_2$, the Fe content directly correlates with the Curie temperature and the lattice parameters can be used to estimate T_C for a given sample. We have demonstrated that large single crystals can be grown out of a self-flux, and neutron diffraction on these crystals confirms ferromagnetic behavior with moments aligned along the c -axis. While these flux grown crystals are Fe-deficient, they are of high quality with regards to diffraction and scattering studies, the latter of which will be performed to investigate the spin waves in this mildly itinerant ferromagnet. Our single crystal diffraction and electron microscopy investigations do not reveal any significant occupation of an interlayer Fe site, though such a site may become occupied at higher Fe content. While we have shown that the magnetic behavior can be controlled through total Fe content, chemical substitutions or intercalation may provide additional control over the magnetism and physical properties of this layered ferromagnetic material. Also, our work points to several areas where theoretical calculations may provide useful information regarding the electronic and magnetic properties of these materials.

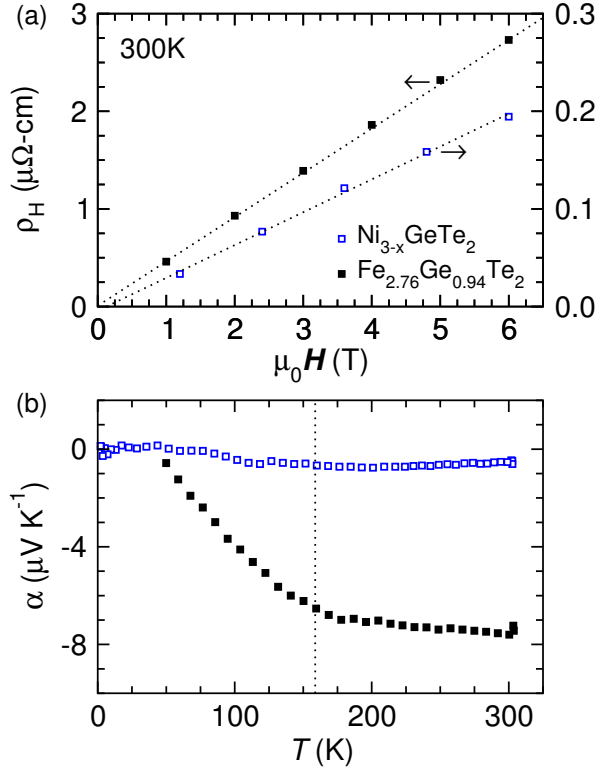


FIG. 10. (color online) (a) Hall resistance as a function of applied field suggests p -type conduction in $\text{Fe}_{2.76}\text{Ge}_{0.94}\text{Te}_2$ and $\text{Ni}_{3-x}\text{GeTe}_2$ crystals, while in (b) the negative Seebeck coefficients indicates n -type conduction. The dashed line in panel (b) indicates the Curie temperature of the $\text{Fe}_{2.76}\text{Ge}_{0.94}\text{Te}_2$ crystal.

V. ACKNOWLEDGEMENTS

This work was supported by the U. S. Department of Energy, Office of Science, Basic Energy Sciences, Materials Sciences and Engineering Division. Research performed at the High Flux Isotope Reactor at Oak Ridge National Lab was supported by the Department of Energy, Scientific User Facility Program. We thank Radu Custelcean for assistance with single crystal x-ray diffraction data collection.

* mayaf@ornl.gov

- ¹ H.-J. Deiseroth, K. Aleksandrov, C. Reiner, L. Kienle, and R. K. Kremer, *Eur. J. Inorg. Chem.* **2006**, 1561 (2006).
- ² B. Chen, J.-H. Yang, H.-D. Wang, M. Imai, H. Ohta, C. Michioka, K. Yoshimura, and M.-H. Fang, *J. Phys. Soc. Jap.* **82**, 124711 (2013).
- ³ S. Z. Butler, S. M. Hollen, L. Cao, Y. Cui, J. A. Gupta, H. R. Gutiérrez, T. F. Heinz, S. S. Hong, J. Huang, A. F. Ismach, E. Johnston-Halperin, M. Kuno, V. V. Plashnitsa, R. D. Robinson, R. S. Ruoff, S. Salahuddin, J. Shan, L. Shi, M. G. Spencer, M. Terrones, W. Windl, and J. E. Goldberger, *ACS Nano* **7**, 2898 (2013).
- ⁴ M. Chhowalla, H. S. Shin, G. Eda, L.-J. Li, K. P. Loh, and H. Zhang, *Nature Chem.* **5**, 263 (2013).
- ⁵ K. Yasukōchi, K. Kanematsu, and T. Ohoyama, *J. Phys. Soc. Jap.* **16**, 429 (1961).
- ⁶ K. Kanematsu, *J. Phys. Soc. Jap.* **20**, 36 (1965).
- ⁷ B. Malaman, J. Steinmetz, and B. Roques, *J. Less-Common Metals* **75**, 155 (1980).
- ⁸ G. M. Sheldrick, *Acta Cryst.* **A64**, 112 (2008).
- ⁹ E. Parthe and L. M. Gelato, *Acta Cryst.* **A40**, 169 (1984).
- ¹⁰ A. L. Spek, *Acta Cryst.* **D65**, 148 (2009).
- ¹¹ J. Rodríguez-Carvajal, *Physica B* **192**, 55 (1993).
- ¹² H. Katsuraki, *J. Phys. Soc. Jap.* **19**, 863 (1964).
- ¹³ E. Germagnoli, C. Lamborizio, S. Mora, and I. Ortalli, *Il Nuovo Cimento* **42B**, 314 (1966).
- ¹⁴ F. Albertini, L. Pareti, A. Deriu, D. Negri, G. Calestani, O. Moze, S. J. Kennedy, and R. Sonntag, *J. Appl. Phys.* **84**, 401 (1998).
- ¹⁵ E. P. Wohlfarth, *J. Mag. Mag. Mater.* **7**, 113 (1978).
- ¹⁶ T. Moriya, *J. Mag. Mag. Mater.* **14**, 1 (1979).
- ¹⁷ See Supplemental Material at [URL will be inserted by publisher] for anomalous Hall effect data, electrical resistivity, thermal transport, and specific heat data.

A. Supplemental Materials

A large number of vacancies are refined on the Fe(2) position from both the neutron and x-ray single crystal diffraction data. When filled, these Fe(2) positions are bonded to three in-plane Ge atoms. As vacancies are introduced, Fe(2)-Ge bonding decreases (on average) and this results in a large in-plane displacement parameter for Ge, as shown in Table III. Consistent with this, we refine a larger concentration of vacancies on Fe(2) compared to Ref. 1, and our refined U_{11} for Ge is also larger

than previously reported. However, the previous study did report a strong anisotropy for the displacement parameters of Ge, and a similar U_{33} to that shown in Table III was reported.¹

The data in Table III correspond to refinement of single crystal x-ray diffraction data, where only Fe(2) was found to be partially occupied. We obtained a fractional occupation of 0.71(2) for Fe(2), and this was utilizing a constraint to maintain equal displacement parameters for Fe(1) and Fe(2). When refined separately, the displacement parameters of Fe(2) are observed to be rather small within the basal plane ($U_{11}=0.004(2)$). However, the occupancy of Fe(2)=0.69(2) is very similar to that obtained from the restrained fit.

With the production of large single crystals, we were able to perform in-plane thermal and thermoelectric transport measurements. Figure 11 presents the electrical resistivity, Seebeck coefficient, and thermal conductivity of our flux-grown $\text{Fe}_{2.76}\text{Ge}_{0.94}\text{Te}_2$ crystals (in-plane transport). This composition is obtained from refinement of single crystal neutron diffraction data. To facilitate a comparison, we have used the composition $\text{Ni}_{2.40}\text{Ge}_{1.01}\text{Te}_{2.00}$ obtained from EDS. The electrical resistivity is about an order of magnitude lower for $\text{Ni}_{2.40}\text{GeTe}_2$ than for $\text{Fe}_{2.76}\text{Ge}_{0.94}\text{Te}_2$ (see caption of Fig. 11). The $\text{Ni}_{2.40}\text{GeTe}_2$ sample also has a slightly lower residual resistivity ratio (RRR), as demonstrated by the plot of $\rho(T)/\rho(300\text{ K})$ in Fig. 11(a). Transition metal vacancies and/or associated displacements of Ge likely provide significant charge carrier scattering that leads to small RRR in both of these systems.

The Seebeck coefficient (α) is small and negative for both samples. The negative value implies electrons dominate conduction, and the smaller value for $\text{Ni}_{2.40}\text{GeTe}_2$ would imply a higher concentration of charge carriers (consistent with lower ρ) or a more complete compensation of electrons/holes. Based on the Hall data discussed below, these appear to be multi-carrier metals.

The estimated lattice thermal conductivity κ_{lat} is similar for $\text{Fe}_{2.76}\text{Ge}_{0.94}\text{Te}_2$ and $\text{Ni}_{2.40}\text{GeTe}_2$, as shown in Fig. 11(c). These κ_{lat} values were obtained using the Wiedemann-Franz law to estimate an electronic contribution κ_e to the total thermal conductivity κ ; the degenerate limit of the Lorenz number was assumed. The values of κ_{lat} are similar across the entire temperature range investigated and a low T maximum is not observed. The temperature dependence suggests vacancies likely dominate phonon scattering rates, and despite apparently different transition metal contents (based on our EDS results) the net result is a similar κ_{lat} . It is also possible that phonons are scattered by charge carriers at low T .

The electrical properties respond to the ferromagnetic ordering in $\text{Fe}_{2.76}\text{Ge}_{0.94}\text{Te}_2$, as observed in Fig. 11(a,b) where the Curie temperature is indicated by the dashed line. Below T_C , the electrical resistivity and Seebeck coefficient also begins to decrease more rapidly. A decrease in ρ below T_C is commonly understood as a reduction in spin disorder scattering when the moments order. The

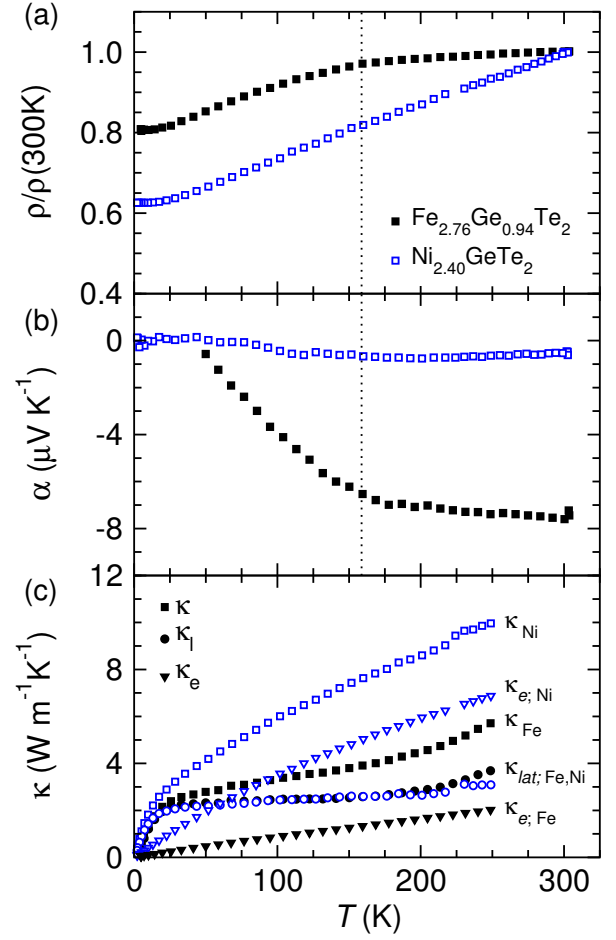


FIG. 11. (color online) In-plane electrical and thermal transport for $\text{Fe}_{2.76}\text{Ge}_{0.94}\text{Te}_2$ and $\text{Ni}_{2.40}\text{GeTe}_2$ crystals. (a) Normalized electrical resistivity, (b) Seebeck coefficient and (c) thermal conductivity with estimates for the lattice and electronic contributions shown. The closed black symbols are for $\text{Fe}_{2.76}\text{Ge}_{0.94}\text{Te}_2$ ($\rho(300\text{ K})=3.0\times 10^{-4}\Omega\text{-cm}$) and the open blue symbols represent $\text{Ni}_{2.40}\text{GeTe}_2$ ($\rho(300\text{ K})=9.50\times 10^{-5}\Omega\text{-cm}$).

source for a decrease in the Seebeck coefficient is less clear. The Seebeck coefficient is influenced by the scattering mechanisms as well as the carrier concentration and shape of the Fermi surface, the latter of which may be influenced by the magnetic ordering. The magnetic scattering may asymmetrically influence the contributions of the various charge carriers, thereby influencing the Seebeck coefficient. We have not noticed a strong response of the lattice to the magnetic ordering in $\text{Fe}_{2.76}\text{Ge}_{0.94}\text{Te}_2$.

We performed Hall effect measurements to further characterize the electrical behavior of these systems. The Hall coefficient is positive for both $\text{Fe}_{2.76}\text{Ge}_{0.94}\text{Te}_2$ and $\text{Ni}_{2.40}\text{GeTe}_2$, and the Hall resistance ρ_H is linear with magnetic fields up to at least 8 T at 300 K (Fig. 12(a)). At room temperature, the Hall coefficient R_H of $\text{Ni}_{2.40}\text{GeTe}_2$ is about an order of magnitude smaller than that of $\text{Fe}_{2.76}\text{Ge}_{0.94}\text{Te}_2$, which translates to a larger carrier concentration in $\text{Ni}_{2.40}\text{GeTe}_2$ if a single-carrier model is

TABLE III. Atomic coordinates and anisotropic displacement parameters for $\text{Fe}_{3-x}\text{GeTe}_2$ from refinements of single crystal x-ray diffraction data at $T=173\text{ K}$.

species	coordinates			$U_{11} = U_{22} = 2U_{12}$	U_{33}	U_{eq}	fractional occupancy
	x	y	z	\AA^2	\AA^2	\AA^2	
Fe(1)	0	0	0.1721(2)	0.0069(12)	0.014(2)	0.0091(10)	1
Fe(2)	1/3	2/3	1/4	0.0069(12)	0.014(2)	0.0091(10)	0.71(2)
Ge	1/3	2/3	3/4	0.044(2)	0.015(2)	0.034(1)	1
Te	1/3	2/3	0.0900(1)	0.0081(6)	0.0152(8)	0.0105(5)	1

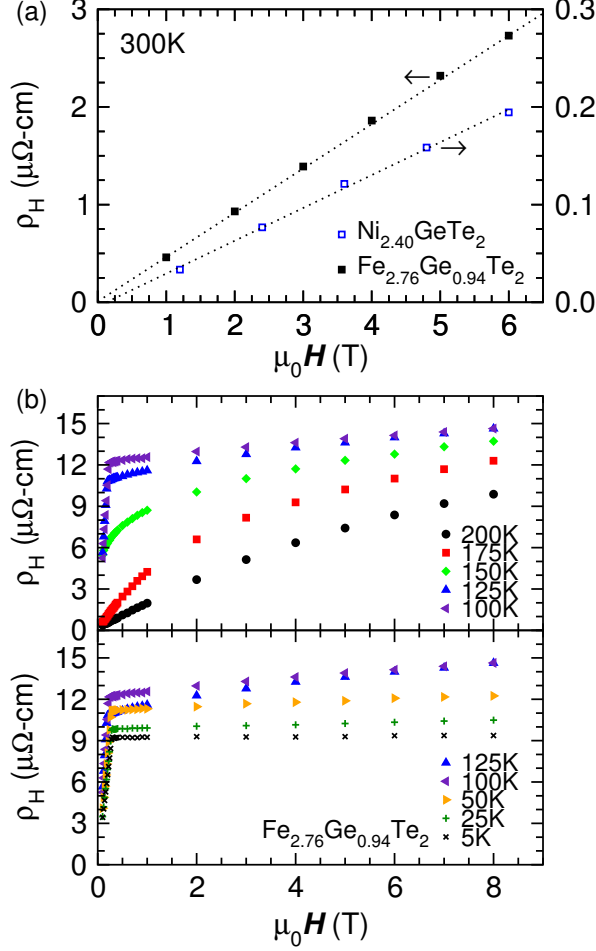


FIG. 12. Hall effect data at (a) 300 K for $\text{Fe}_{2.76}\text{Ge}_{0.94}\text{Te}_2$ and $\text{Ni}_{2.40}\text{GeTe}_2$ and in (b,c) the influence of an anomalous component brought about by the ferromagnetic ordering in $\text{Fe}_{2.76}\text{Ge}_{0.94}\text{Te}_2$ is demonstrated.

used. Specifically, at 300 K the Hall carrier density $n_H = 1/R_{\text{He}}$ is $\approx 1.8 \times 10^{22} \text{ cm}^{-3}$ for $\text{Ni}_{2.40}\text{GeTe}_2$ and $\approx 1.4 \times 10^{22} \text{ cm}^{-3}$ for $\text{Fe}_{2.76}\text{Ge}_{0.94}\text{Te}_2$ using the linear fits shown in Figure 12(a).

The positive Hall coefficient suggests the dominant carriers are holes while the negative sign of the Seebeck coefficient suggests the dominant charge carriers are electrons. A detailed analysis of the contributions of each band is prohibited, however, due to the linearity of the Hall resistance with magnetic field. If both holes and

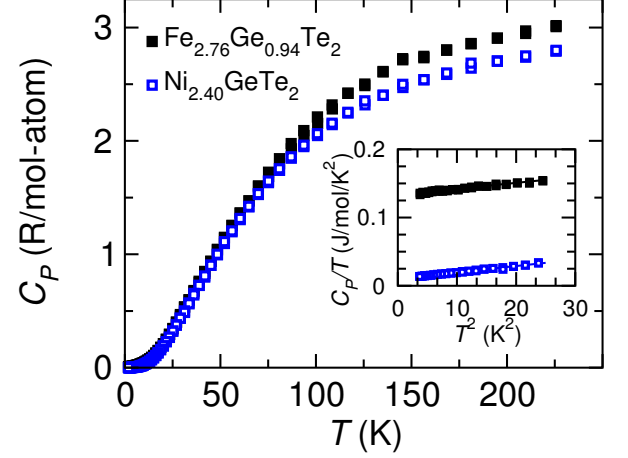


FIG. 13. (color online). Specific heat capacity of $\text{Fe}_{2.76}\text{Ge}_{0.94}\text{Te}_2$ and $\text{Ni}_{2.40}\text{GeTe}_2$, with inset showing low T behavior and fits (thin solid lines). A small anomaly is observed in $\text{Fe}_{2.76}\text{Ge}_{0.94}\text{Te}_2$ near $T_C \approx 150\text{ K}$.

electrons are present, as suggested by these results, the Hall coefficients could be artificially reduced and the carrier concentrations reported would be upper-limits to the actual number of holes in the system. $\text{Ni}_{2.40}\text{GeTe}_2$ is more conductive, despite apparently having more defects, and thus an increase in the absolute number of charge carriers relative to $\text{Fe}_{2.76}\text{Ge}_{0.94}\text{Te}_2$ is likely.

The Hall effect of $\text{Fe}_{2.76}\text{Ge}_{0.94}\text{Te}_2$ is strongly influenced by the anomalous Hall contribution, as shown in Fig. 12(b,c). For our crystals, with a Curie temperature of $\approx 150\text{ K}$, an influence of the anomalous Hall effect is observed below approximately 200 K. This is due to the strong polarization of the Fe moments with increasing field and decreasing temperature. The Hall data follow the field dependence of the magnetization, which demonstrates that the non-linearity of ρ_H is not due to multi-band effects. The regular and anomalous Hall coefficients have the same sign, and the current data are insufficient to analyze in detail due to the small contribution from the regular Hall coefficient as well as the non-saturating magnetization at high fields. Qualitatively different results were obtained for the regular Hall coefficient when a detailed analysis was performed on data collected for different crystals, which had similar room temperature Hall coefficients (likely due to minor variations in magnetization between the crystals).

Specific heat measurements were performed on single crystals of $\text{Fe}_{2.76}\text{Ge}_{0.94}\text{Te}_2$ and $\text{Ni}_{2.40}\text{GeTe}_2$, and the results are shown in Fig. 13. A small anomaly is present in the region of the ferromagnetic transition of $\text{Fe}_{2.76}\text{Ge}_{0.94}\text{Te}_2$ while data for $\text{Ni}_{2.40}\text{GeTe}_2$ are smooth across the entire temperature range. The measured values are approaching the high temperature limit of $3k_B/\text{atom}$ at 220 K for both materials. This is consistent with the Debye temperatures obtained from the low T data, which were $\Theta_D=224$ K and 234 K for $\text{Ni}_{2.40}\text{GeTe}_2$ and $\text{Fe}_{2.76}\text{Ge}_{0.94}\text{Te}_2$, respectively. The slightly smaller Θ_D for $\text{Ni}_{2.40}\text{GeTe}_2$ could be due to increased softening associated with a higher carrier density or a higher vacancy concentration, though potential error associated with the sample compositions precludes such a conclu-

sion. At low temperatures, the Debye temperature Θ_D is obtained from a plot of C_P/T versus T^2 plot where the slope is $\frac{12\pi^4 R N_{at}}{5\Theta_D^3}$ and N_{at} is the number of atoms per formula unit.

The electronic coefficient to the specific heat is significantly larger for $\text{Fe}_{2.76}\text{Ge}_{0.94}\text{Te}_2$ than for $\text{Ni}_{2.40}\text{GeTe}_2$. We obtain a Sommerfeld coefficient $\gamma = 132.8 \text{ mJ/mol/K}^2$ for $\text{Fe}_{2.76}\text{Ge}_{0.94}\text{Te}_2$ and 10.2 mJ/mol/K^2 for $\text{Ni}_{2.40}\text{GeTe}_2$. The large γ for $\text{Fe}_{2.76}\text{Ge}_{0.94}\text{Te}_2$ is either due to a mass enhancement from correlations or due to a contribution from spin fluctuations. We note that our γ is similar to that reported for vapor transport grown Fe_3GeTe_2 crystals.²